Geochemistry, Geophysics, Geosystems

RESEARCH ARTICLE
10.1029/2021GC009715

Teleseismic *P*-Wave Attenuation Beneath the Southeastern United States

Ashutosh Shrivastava[1], Kelly H. Liu[1], and Stephen S. Gao[1]

[1]Geology and Geophysics Program, Missouri University of Science and Technology, Rolla, MO, USA

Key Points:

- Crustal and upper mantle *P*-wave attenuation is measured at 477 USArray and other stations in SE USA by linear fitting of spectral ratios
- The Gulf of Mexico Coastal Plain possesses anomalously low attenuation that is attributable to stagnant fossil lithosphere
- Scattering contributes a small fraction of the observed attenuation, and is less strong in the Coastal Plain than the rest of the area

Supporting Information:

Supporting Information may be found in the online version of this article.

Correspondence to:

Kelly H. Liu,
liukh@mst.edu

Citation:

Shrivastava, A., Liu, K. H., & Gao, S. S. (2021). Teleseismic *P*-wave attenuation beneath the southeastern United States. *Geochemistry, Geophysics, Geosystems*, *22*, e2021GC009715. https://doi.org/10.1029/2021GC009715

Received 11 FEB 2021
Accepted 2 JUN 2021

Abstract Seismic attenuation is an important parameter for characterizing subsurface morphology and thermal structure. In this study, we use *P*-wave amplitude spectra from 588 teleseismic events recorded by 477 broadband seismic stations in the southeastern United States to examine the spatial variations of seismic attenuation in the crust and upper mantle. The resulting seismic attenuation parameter (Δt^*) measurements obtained using the spectral ratio technique reveal a zone of relatively low attenuation in the Gulf of Mexico Coastal Plain and the southwestern terminus of the Piedmont province. Spatial coherency analysis of the Δt^* observations suggests that the center of the low attenuation layer is located within the uppermost mantle at about 70 km depth. This low attenuation anomaly lies along the suture zone between Laurentia and Gondwana and approximately coincides with the east-west trending Brunswick magnetic anomaly. The origin of this low attenuation anomaly can be attributed to low attenuation bodies in the form of remnant lithospheric fragments in the deep crust and the uppermost mantle. The contribution of scattering to the observed Δt^* is estimated by calculating the ratio of amplitude on the transverse and vertical components in the *P*-wave window. Relative to the rest of the study area, the Gulf of Mexico Coastal Plain demonstrates weaker scattering which is suggestive of a more homogenous crustal and uppermost mantle structure.

1. Introduction

Seismic attenuation is an important physical parameter for characterizing rocks and providing significant constraints on the viscosity, rigidity, temperature, and mineral composition of the Earth's crust and mantle (Jackson & Anderson, 1970; Knopoff, 1964). Additionally, seismic attenuation measurements can provide independent constraints on the interpretation of seismic velocity models (Deen et al., 2006; Faul & Jackson, 2005; Godey et al., 2004; Goes & van der Lee, 2002; Goes et al., 2000; Hwang et al., 2009; Lee, 2003; Schutt & Lesher, 2006; Shapiro & Ritzwoller, 2004; Sobolev et al., 1996). Previous seismological investigations suggest that anelasticity and velocity variations exhibit strong sensitivity to temperature anomalies in the uppermost mantle (Anderson, 1967; Faul & Jackson, 2005; Goes et al., 2000; Jackson et al., 2002; Karato, 1993; Knopoff, 1964; Sato et al., 1989; Wang et al., 2017). Such anelasticity can be estimated by measuring the attenuation of teleseismic body waves, as they provide frequencies intermediate to those of long-period surface waves and regional earthquake body waves (Solomon, 1972; Wang et al., 2017).

Anelastic or intrinsic attenuation refers to the conversion of seismic energy into heat, generally caused by grain boundary friction (Jackson & Anderson, 1970) and the movements of dislocations through the mineral grains (Gorich & Muller, 1987). Anelastic attenuation of seismic waves in a medium is expressed in terms of the seismic quality factor (Q), which is inversely proportional to anelastic attenuation. The relation between Q and energy dissipation is

$$Q = 2\pi \frac{Eo}{\delta E}, \tag{1}$$

where E_o is the maximum value of elastic energy stored during one cycle of loading, and δE is the energy loss during the cycle (Knopoff, 1964).

In addition to anelasticity, scattering can also lead to the reduction of body-wave amplitude. Akinci et al. (1995) propose that the energy dissipation of body waves due to scattering is more prominent at shorter distances and decreases substantially as the propagation distance increases. The study also suggests that

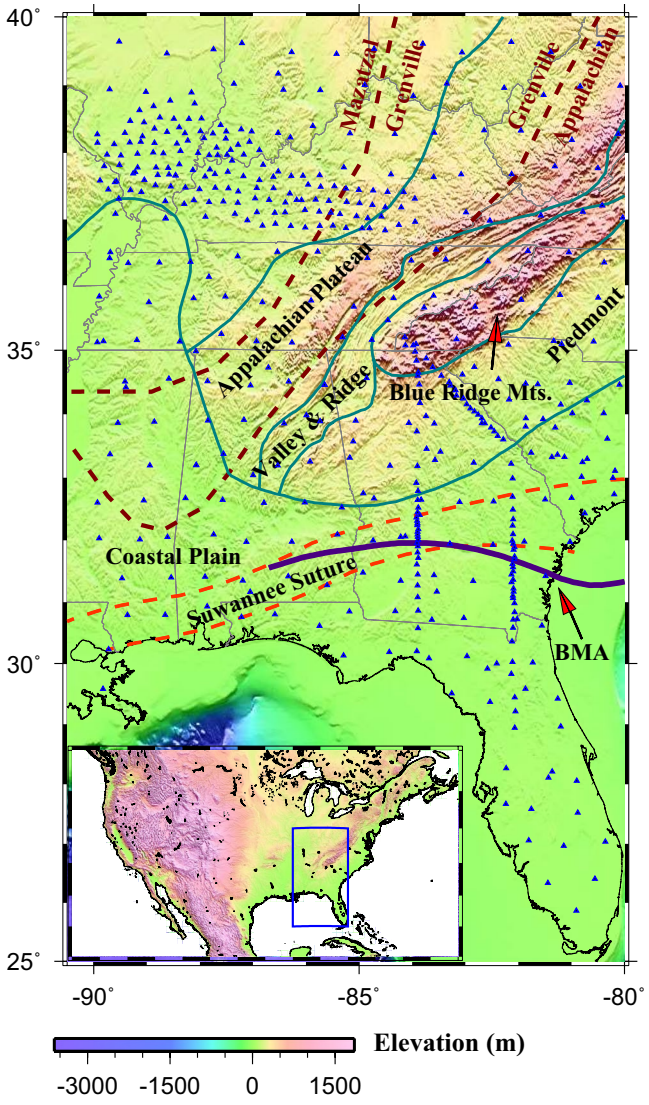

Figure 1. Topographic map of the study area showing the location of seismic stations (blue triangles), physiographic boundaries (teal solid lines), Precambrian basement terrane boundaries (maroon dashed lines), Suwannee Suture Zone (Mueller et al., 2014; orange dashed lines), and the path of the Brunswick Magnetic Anomaly (BMA; Mueller et al., 2014; purple line). The inset in the figure shows the location of the study area marked by the blue rectangle.

intrinsic attenuation is dominant at larger epicentral distances, without showing a strong frequency dependence. Laboratory experiments have also reported frequency-independent Q for many solids up to moderately high frequencies (Knopoff, 1964). On the basis of previous laboratory and observational studies (Dziewonski, 1979; Jackson & Anderson, 1970; Knopoff, 1964), frequency-independent Q is assumed in this and numerous previous studies (e.g., Hwang et al., 2009) to estimate the attenuation of teleseismic P-waves for frequencies up to 1 Hz.

The southeastern United States (SEUS) is tectonically more stable than the western U.S. but is more active than most portions of the central U.S. (Figure 1). Since the late Proterozoic (>1.0 Ga), multiple phases of terrane accretion, orogenies, and continental breakups have taken place in the SEUS (Cook et al., 1979; Hatcher, 2010; Thomas, 2006). The Grenville orogeny is the oldest known Mesoproterozoic mountain-building episode that marks the assembly of the supercontinent Rodinia (~1.1 Ga; Denison et al., 1984; Thomas, 1985). The Grenville Front separates the SEUS continental margin from the Mazatzal province (Figure 1), which was formed due to the accretion of juvenile volcanic arcs to the older stable core of North America. Following the breakup of Rodinia (~570 Ma), several episodes of continental accretion and orogenies resulted in the formation of the SEUS terrane. The Alleghanian orogeny represented by the collision of Laurentia and Gondwana at ~330 Ma resulted in the formation of the supercontinent Pangea (Iverson & Smithson, 1983; Rankin et al., 1991). This collision marked the formation of the Appalachian Mountains and the addition of the Suwannee terrane, which has significantly different tectonic attributes, lithology, and fossil accumulations than Laurentia (Mueller et al., 2014). A regionally extensive swath of lower-than-normal magnetism known as the Brunswick Magnetic Anomaly (BMA; Figure 1) lines up with the Suwannee Suture zone (Higgins & Zietz, 1983; Mueller et al., 2014; Williams & Hatcher, 1983).

The attenuation structure from previous continental-scale studies in North America suggests relatively low attenuation in the eastern and southeastern U.S. in comparison to the tectonically active western U.S. (Der et al., 1982; Der & McElfresh, 1977; Hwang et al., 2009; Lawrence et al., 2006; Solomon & Toksöz, 1970). A recent study (Cafferky & Schmandt, 2015) computes the spatial variation of seismic attenuation across the U.S. using teleseismic P-wave spectra from deep earthquakes for multiple frequency bands between 0.08 and 2 Hz. All frequency bands yield a high attenuation region near the Appalachian margin and low to medium attenuation is reported in the continental interior. Most of the previous seismic attenuation studies are conducted for the entire continental U.S. with a limited spatial resolution in the SEUS. In this study, a comprehensive assessment of seismic attenuation and the effects of scattering beneath the SEUS is conducted using data from the USArray and other portable or permanent deployments listed in the Data Availability Statement section. The results support the existence of remnant lithospheric segments in the crust and upper mantle beneath the Gulf of Mexico (GoM) Coastal Plain.

2. Data and Methods

Seismic data used in the study were recorded by 477 broadband seismic stations and were obtained (Figure 1) from the Incorporated Research Institutions for Seismology (IRIS) Data Management Center (DMC). The stations include 220 USArray Transportable Array (TA) stations which sampled the study area with ~70 km spacing. The cutoff magnitude (M_c) for data requesting is computed using

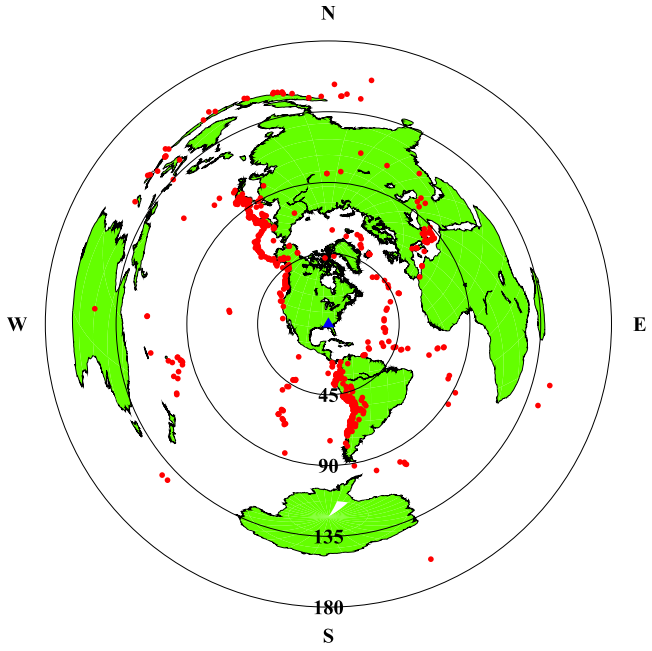

Figure 2. An azimuthal equidistant projection map centered at the study area showing the teleseismic events (red dots) used in this study. The concentric circles represent the distances (in degree) from the center of the study area (blue triangle).

$M_c = 5.2 + (\Delta - \Delta_{min})/(180.0 - \Delta_{min}) - D/D_{max}$, where Δ is the epicentral distance (which ranges from 30° to 180°) in degree, D is the focal depth in km, $\Delta_{min} = 30°$, and $D_{max} = 700$ km (Liu & Gao, 2010). The events were recorded by both portable and permanent seismic stations in the area of 25°–40° North and 80°–90° West, between March 1993 and January 2019. To enhance the quality of the measurements, only events recorded by a minimum of 10 stations were kept, and as a result, 588 teleseismic events (Figure 2) were used in the study.

Several techniques have been developed to estimate the amplitude of seismic attenuation. These techniques can be broadly classified as either time-domain methods or frequency domain methods. Wavelet modeling (Jannsen et al., 1985), rise-time (Gladwin & Stacey, 1974), and analytical signal (Taner et al., 1979) methods are some of the major techniques used to compute seismic attenuation in the time domain, whereas methods such as spectral ratio (Teng, 1968), spectral matching (Raikes & White, 1984), coda normalization (Aki, 1980), and spectral modeling (Gao, 1997; Halderman & Davis, 1991) work in the frequency domain.

Attenuation is measured in terms of the attenuation parameter t*, which is defined as the total traveltime of the wave along the raypath divided by the quality factor (Kovach & Anderson, 1964), that is,

$$t^* = \int_{ray} \frac{1}{V(r)Q(r)} ds, \tag{2}$$

where $V(r)$ is the velocity of the waves, and $Q(r)$ is the quality factor.

In the frequency domain, the amplitude spectrum $A_{ik}(f)$ of an event "k" recorded at station "i" can be expressed as (Teng, 1968)

$$A_{ik}(f) = S_k(f) G_{ik}(f) R_{ik}(f) I_i(f), \tag{3}$$

where $S_k(f)$ is the source spectrum of the source wavelet, $R_{ik}(f)$ is the spectrum of the near-receiver effects, $I_i(f)$ is the spectrum of the instrument response, and $G_{ik}(f)$ is the spectrum of Green's function, which can be written as

$$G_{ik}(f) = e^{-\pi f t^*_{ik}(f)}. \tag{4}$$

The spectral ratio method used in the study is the most widely used technique to estimate seismic body-wave attenuation relative to a reference spectrum (e.g., Der & McElfresh, 1976; Hwang et al., 2009; Solomon & Toksöz, 1970; Teng, 1968). One of the benefits of using this method is that for teleseismic events, the source signal and common path effects are removed. The requested vertical component seismograms are re-sampled into a sampling frequency of 20 sps, and a section of the vertical component seismogram with a total length of 51.2 s (i.e., 1024 data samples) starting from 10 s before the theoretical arrival time of the *P* (or *PKP*) is selected for computing the spectrum. The instrument response is removed by deconvolving the seismograms with the instrument response function. A 10-s window length before the arrival of *P*-wave is used to determine the noise amplitude. The signal-to-noise ratio (SNR) between the maximum absolute value of the signal amplitude and mean absolute noise amplitude is computed for every trace, and seismograms with an SNR smaller than 10.0 are not used for the study. The *P*-wave section of the seismogram is tapered using the customary cosine-sum window, with the form

$$w(n) = a_0 - (1 - a_0)\cos\frac{2\pi n}{N}, 0 \le n \le N, \tag{5}$$

where $w(n)$ is a zero-phase function, N is a positive integer, and the numerical value of a_0 is set as 0.54, which categorizes this tapering function as a Hamming window. A bandpass filter with corner frequencies of 0.1 and 0.5 Hz is applied to the selected seismograms. Amplitude spectra of all the filtered high-quality seismograms are computed using the Fourier transform. To minimize the effects of heterogeneities outside the study area, for each event we use the mean spectrum computed over all the stations that recorded this event as the reference spectrum in the spectral ratio. Additionally, to exclude seismograms with high noise, the minimum correlation coefficient between each spectrum and the mean spectrum is set to 0.9. The relative attenuation factor Δt^*_{ik} between station "i" and the reference spectrum from event "k" is calculated by fitting the spectral ratio with a straight line using the least-squares method (Der & McElfresh, 1977; Solomon & Toksöz, 1970), that is,

$$\ln \frac{A_i(f)}{A_k(f)} = C - \pi \, \Delta t^*_{ik} \, f, \tag{6}$$

where C is the ratio between the near receiver effects of station "i" and the reference spectrum from event "k" ($R_{ik}(f)$ in Equation 3) and is assumed to be frequency independent. The automatically computed results are then manually checked to remove measurements with abnormal data or with a nonlinear frequency variation of the spectral ratios. Furthermore, Δt^*_{ik} measurements with an absolute value greater than 1.0 s, or a standard deviation greater than 0.2 s are excluded. Figure 3 shows an example of the spectral ratio and associated spectra and seismograms.

3. Results

The resulting 14,702 individual Δt* measurements (Figure 4a) obtained using the spectral ratio method are used to compute the station-averaged Δt* measurements if the number of measurements obtained at the station is three or greater (Figures 4b and 5a and Table S1), which vary from −0.62 s ± 0.03 to 0.60 s ± 0.04 s in the study area and demonstrate systematic spatial variations. The station-averaged Δt* measurements (Figure 5a) are spatially interpolated by averaging the measurements in overlapping 1° by 1° blocks with a moving step of 0.1° (Figure 5b). We experimented with different values of the size of the blocks for smoothing and found 1° to be a balanced value that most clearly demonstrates the spatial variation of station averaged Δt* measurements. As the block size for smoothing increases, both the spatial resolution and peak-to-peak range of the Δt* measurements decrease, and vice versa. To get a sense of the uncertainties in the Δt* measurements, we compute the spatial distribution of the standard deviation (SD) of the Δt* measurements (Figure 6). Areas with the largest SD are in the Florida Peninsula and along the southernmost part of the GoM Coastal Plain. Some previous studies (e.g., Cafferky & Schmandt, 2015; Dong & Menke, 2017) used only events with hypocenters deeper than at least 150 km for attenuation measurements for the purpose of reducing the impact of the reduction in high frequency components by the lithosphere on the source-side. To explore the influence of including the shallow events, we compute Δt* measurements by only using events with a focal depth ≥150 km. The results (Figure S1) show similar spatial variations with those obtained using all the events (Figure 5), even with a much-reduced number of measurements.

Based on the characteristics of the measurements (Figure 5) and the tectonic setting, we divide the study area into five areas: Mazatzal Province (A), Grenville Province (B), Southern Appalachian Mountain Range and Piedmont Province (C), GoM Coastal Plain (D), and Florida Peninsula (E). Area A is part of the stable central North American craton and is characterized by positive V_p anomalies in the upper-most mantle (Figure 5a; Golos et al., 2020). Physiographically, the eastern portion of Area A belongs to the Appalachian Plateau, located adjacent to the southern end of the Appalachian Mountains. The southeastern region of the area displays higher attenuation relative to other regions in the area. The western portion of Area A consists of the Interior Lowlands that include several structural depressions that have filled with sediments mostly eroded from the mountains (Swaby et al., 2016). Attenuation decreases gradually westward as the lithospheric thickness beneath the stable part of North America Craton increases. The northwestern region of Area A consists of the Illinois Basin comprising of a thick layer of Cambrian through Pennsylvanian sedimentary rocks (Swann, 1968) and Proterozoic granites and rhyolite in the basement which date back to around 1.55 Ga (van der Pluijm & Catacosinos, 1996; van Schmus et al., 2007). Negative Δt* measurements

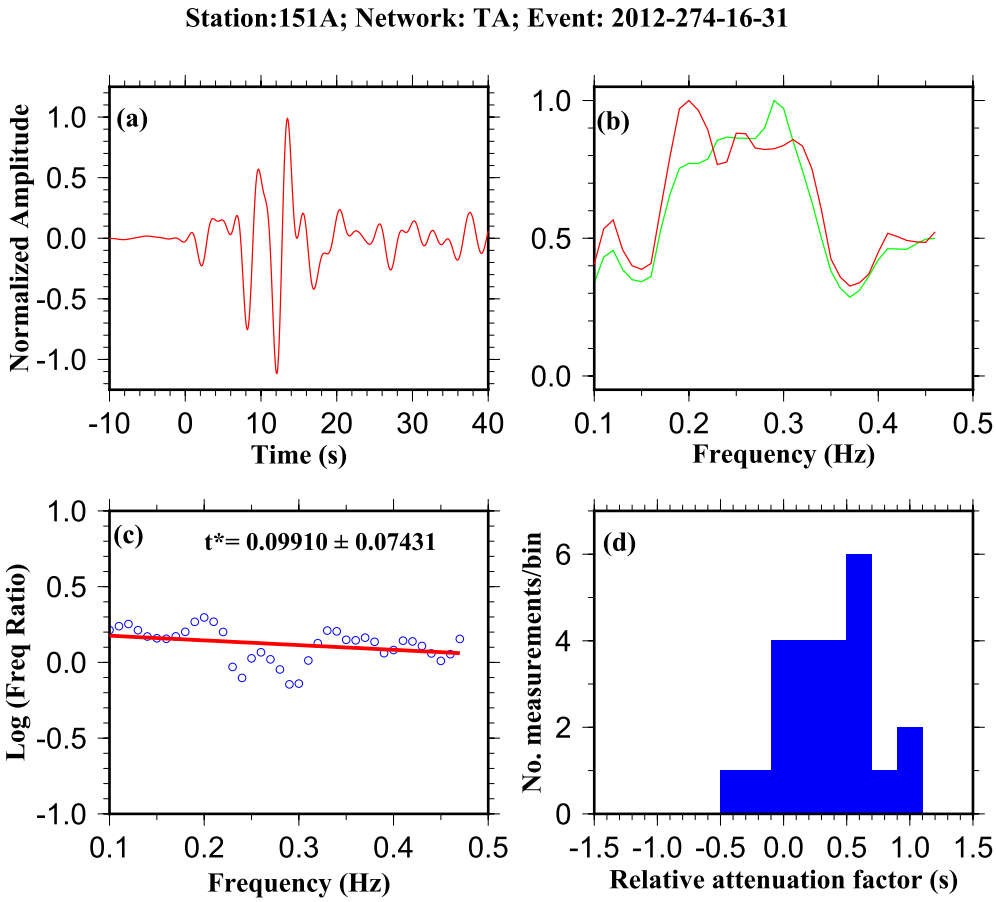

Figure 3. An example of spectral ratio analysis for TA station 151A. (a) Normalized *P* waveform for TA station 151A for event 2012-274-16-31 with an epicentral distance of 31.6°. (b) Normalized spectra for the time series shown in (a) (red), and the mean spectrum (green). (c) The spectral ratio between Station 151A and the mean spectrum plotted against frequency. The red line represents the line of best fit. (d) Histogram of Δt* measurements for all the events recorded by Station 151A.

obtained in the Illinois Basin coincide with the strong positive V_p anomaly mapped by Golos et al. (2020) that extends up to the depth of 70 km. The southernmost tip of Area A is characterized by negative Δt* observations belonging to a zone of low attenuation pervasively observed along the northern border of the GoM Coastal Plain (Figure 5). The average Δt* value for Area A is close to zero (0.01 s ± 0.01 s).

Area B occupies the Grenville Province tectonically and is composed of the Appalachian Plateau except for the southernmost quarter which belongs to the GoM Coastal Plain. The observed Δt* values show a sharp contrast between the Appalachian Plateau and the GoM Coastal Plain, with mean values of 0.03 s ± 0.01 s for the former, and −0.30 s ± 0.03 s for the latter region. The NE portion of the area, which is found to possess high V_P anomalies in the uppermost mantle (Figure 5a), shows reduced Δt* measurements. The SW boundary of Area B traverses the area with negative Δt* values, suggesting that the observed spatial variation of the Δt* measurements is not controlled by Precambrian basement terranes, but by physiographic divisions which are mostly the result of post-Precambrian tectonic activities.

Area C is a physiographical province mostly consisting of the Blue Ridge Mountains and Valley and Ridge of the southern Appalachian Mountains in the west, and a plateau region of the Piedmont Province in the east. Although the western and the eastern regions of Area C are physiographically distinct from each other, both regions share similar crystalline igneous and metamorphic rocks (Swaby et al., 2016). The northernmost part of this area is comprised of the Appalachian Plateau. Similar to Areas D and E, tectonically it is part of the Paleozoic-Cenozoic Appalachian Province. The Δt* measurements are comparable to Area B, with an areal mean value of 0.16 s ± 0.01 s but are higher than those observed on the GoM Coastal Plain

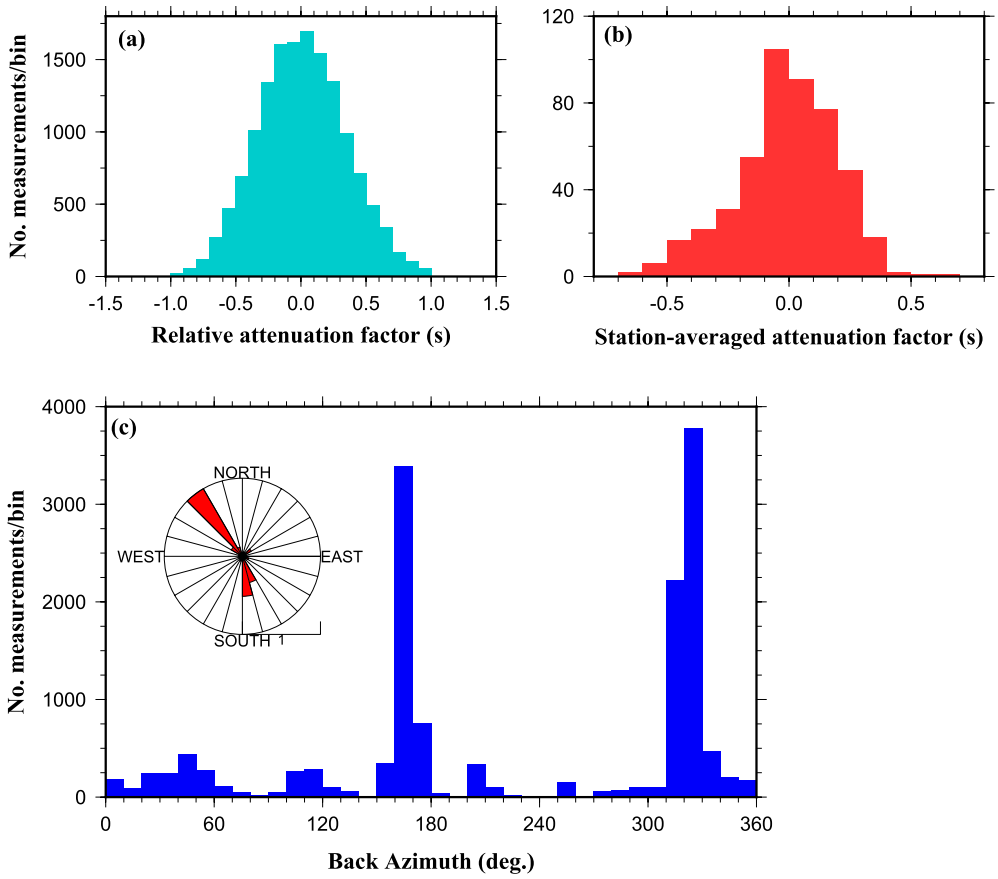

Figure 4. Distribution of (a) Δt* measurements for all events and (b) station-averaged Δt* measurements. (c) Azimuthal distribution of the individual Δt* measurements.

(Figure 5). No obvious change in Δt* is observed across the boundary between this area and Area B, which is a tectonic boundary.

Area D belongs to the GoM Coastal Plain, which is composed of very young rocks, ranging in age from the Cretaceous to the present. It is characterized by a well-defined E-W zone of low Δt* measurements, except for the NE and SW corners of the area. The zone of negative Δt* closely follows the northern boundary of the GoM Coastal Plain and extends to the southernmost portions of Areas A and B. The mean Δt* value for this area is −0.17 s ± 0.02 s which is the lowest among all the five areas.

Area E, which includes the Florida Peninsula, is characterized by Δt* values that are intermittent between those observed in Areas A–C and D, with a mean value of −0.03 s ± 0.02 s. The Δt* values demonstrate a southward gradual increase (Figure 5a), and the same trend is observed for the uncertainty of the measurements (Figure 6).

We estimate the optimal depth of the observed Δt* anomalies by adapting a procedure that was developed for estimating the depth of the source of anisotropy using shear wave splitting measurements (Liu & Gao, 2011). Spatial coherency of seismic attenuation parameters is used to estimate the depth of seismic attenuation by computing a spatial variation factor ($F_{\Delta t}$). The geometric distribution of the ray-piercing points is computed at a depth incremental interval of 5 km from 0 to 400 km, based on the IASP91 Earth model (Kennett & Engdahl, 1991). For each depth, the study area is divided into overlapping blocks of 0.2° × 0.2° at a distance of 0.05° between the centers of the neighboring blocks. $F_{\Delta t}$ values are then calculated at each depth using

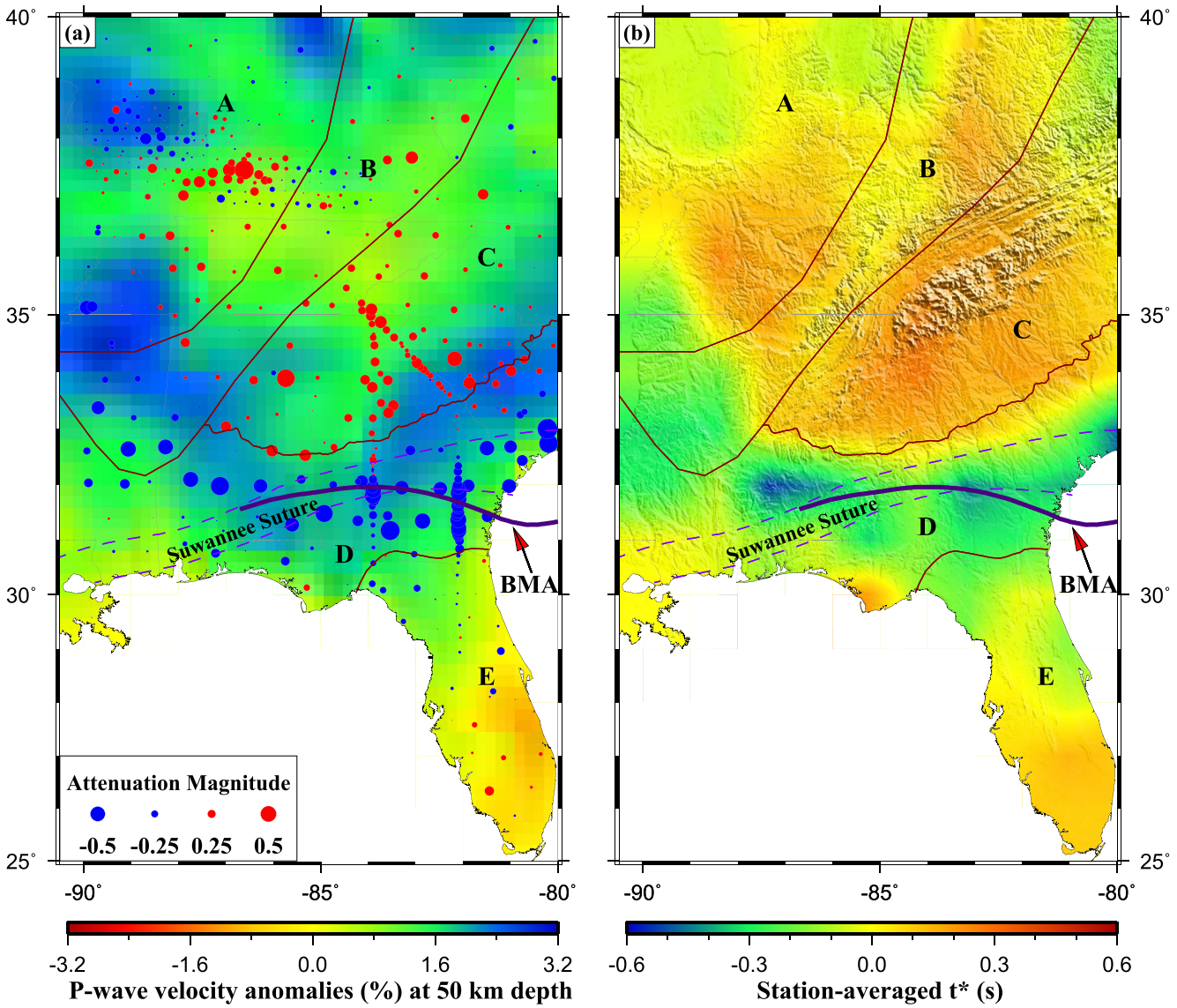

Figure 5. (a) Station-averaged *P*-wave attenuation factors (circles) plotted on a background of *P*-wave velocity anomalies (%) at 50 km depth (Golos et al., 2020). Maroon lines represent the boundaries of five regions, divided based on the characteristics of the measurements and the tectonic setting. (b) Spatially averaged *P*-wave attenuation factors.

$$F_{\Delta t} = \frac{1}{\mathrm{N}} \sum_{i=1}^{N} \sqrt{\frac{1}{Mi-1} \sum_{j=1}^{Mi} \left(\Delta t_{ij} - \overline{\Delta t_i}\right)^2}, \tag{7}$$

where N is the number of blocks, M_i is the number of measurements for the i-th block, Δt_{ij} is the attenuation parameter in the i-th block, and $\overline{\Delta t_i}$ is the average Δt* over all the measurements in block i. A detailed explanation of this approach along with the FORTRAN program is illustrated in Gao & Liu (2012). The assumption adopted in this approach is that the attenuation of body waves is caused by a single horizontal layer with spatially variable thickness. This means that the resulting optimal depth corresponding to the minimum value of $F_{\Delta t}$ indicates the center of the layer. Figure 7 shows the calculated $F_{\Delta t}$ plotted against the assumed depth of attenuation for the SEUS. The resulting $F_{\Delta t}$ shows that the optimal depth is about 70 km, that is, in the uppermost mantle. Note that the optimal depth can be viewed as the weighted mean depth computed by the magnitude of lateral variations of the observed Δt* values. For a homogenous layer, it is

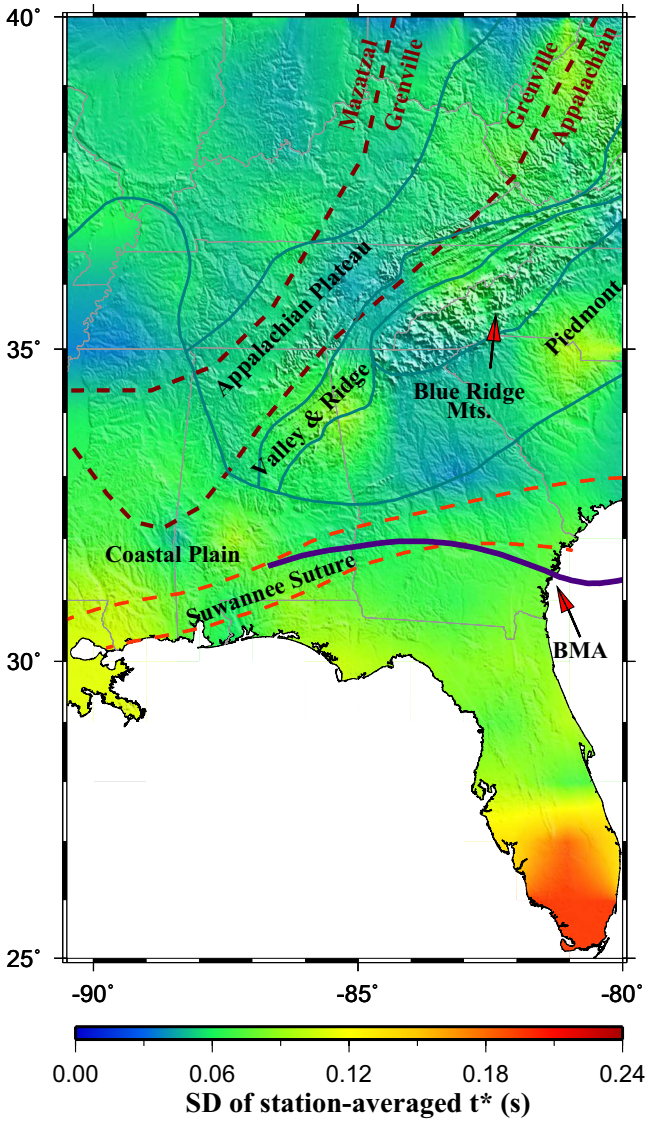

Figure 6. Distribution of the standard deviation of station averaged *P*-wave attenuation factors.

the depth of the center of the layer. If Δt* variations decrease with depth, the resulting optimal depth is smaller than the center of layer and vice versa. In all cases, the actual thickness of the layer cannot be determined.

4. Discussion

4.1. Comparisons With Previous Seismic Wave Attenuation and Velocity Tomography Studies

Previous larger-scale body wave (Cafferky & Schmandt, 2015; Hwang et al., 2009; Solomon & Toksöz, 1970) and surface wave (Bao et al., 2016; Baqer & Mitchell, 1999; Pasyanos, 2013) attenuation studies show a common pattern of high attenuation in the Appalachian Mountains and low attenuation beneath the GoM Coastal Plain. Cafferky & Schmandt (2015) map the upper mantle Δt* values across the contiguous U.S. by inverting teleseismic *P*-wave amplitude spectra for multiple frequency bands ranging between 0.08 and 2 Hz. The Δt* values obtained for all the frequency bands are consistent with the results obtained in this study. Cafferky & Schmandt (2015) display the Δt* measurements using a median smoothing radius of 1.75° and 5° that resulted in two different spatial resolutions. The spatially interpolated results from this study (Figure 5b) are obtained by overlapping 1° by 1° blocks and are similar to their results obtained using the median smoothing radius of 1.75°. They report the lowest mean 95% confidence interval of Δt* measurements (0.09 s) for the 0.08–2 Hz band, and highest (0.21 s) for the 0.08–0.5 Hz band calculated using over 16,000 Δt* measurements across the entire contiguous U.S. In comparison, the 95% confidence interval of 14,702 Δt* measurements in our study is 0.01 s for the SEUS. Note that in our study the frequency band is 0.1–0.5 Hz, where the teleseismic *P*-wave is the strongest (Figure 3b) which could account for the differences in the small confidence interval of our measurements.

A surface wave attenuation study (Gallegos et al., 2014) uses a two-station method to estimate *Lg* attenuation in the central and eastern U.S. Their results reveal a low crustal attenuation anomaly beneath the GoM Coastal Plain, which correlates with the location of the low attenuation anomaly observed in our study. Lawrence et al. (2006) measure seismic attenuation beneath the North American continent using waveform cluster analysis and further correlate the results with the travel time. The study finds that seismic travel times and attenuation are weakly correlated ($R^2 < 0.3$). The sparsely populated seismic stations over a large study area and decreased waveform coherence between the stations produced large-scale variations in seismic attenuation, and therefore, the attenuation structure in the SEUS is mapped with a low spatial resolution relative to those using data from the USArray. Other previous studies (Der et al., 1982; Der & McElfresh, 1977; Hwang et al., 2009; Solomon & Toksöz, 1970) calculate the crustal and upper mantle seismic attenuation beneath the U.S., and none of them reveals the low attenuation anomaly observed in our results near the southwestern terminus of Piedmont (Figure 5b). This is possibly due to the limited number of stations used in most of these studies to produce continent-scale attenuation maps, hence unable to resolve detailed features, and only major trends are reported. Our results make a more comprehensive assessment of *P*-wave attenuation using a large number of waveforms thereby obtaining a more detailed attenuation structure of the SEUS.

We next compare our results with those from previous velocity tomography studies to provide constraints on the geological implications of the attenuation measurements. The shear velocity in the upper mantle beneath the study area is as much as 15%–20% higher than that in the western U.S. as reported in the studies of body wave travel-times (Golos et al., 2018; Grand & Helmberger, 1984; Melbourne & Helmberger, 1998)

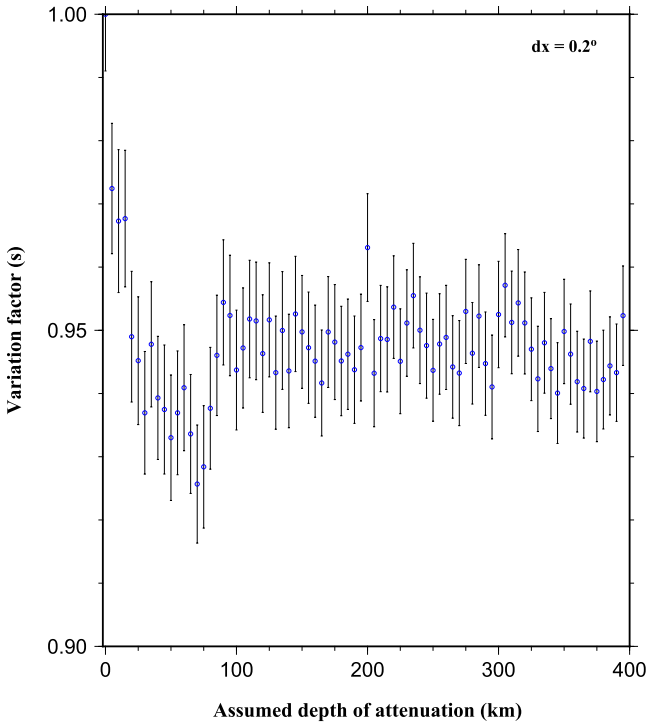

Figure 7. Depth of the source of attenuation estimated using the approach of Gao & Liu (2012) with a bin size (dx) of 0.2°.

and surface wave dispersion (Marone & Romanowicz, 2007; van der Lee & Nolet, 1997). Golos et al. (2018) estimate the variations in shear wave speed anomalies in the crust and upper mantle using data from the USArray and permanent seismic networks in the continental U.S. Their body wave inversion results indicate low wave speeds beneath the Appalachian Mountains which correlate with the high attenuation observed in Areas B and C in our study. These low wave speed anomalies are confined in the depth range between 40 and 60 km, as inferred from the surface wave inversion results. Another study (Shen & Ritzwoller, 2016) estimates similar low-velocity anomalies in the mantle beneath the Appalachians in western Virginia. Some of the recent studies (Biryol et al., 2016; Golos et al., 2020; Wang et al., 2019) map the 3-D *P*-wave velocity structure of the crust and upper mantle beneath the southeastern U.S. using the travel-time residuals from teleseismic *P*-wave data. Biryol et al. (2016) report high-velocity anomalies beneath the GoM Coastal Plain in the upper-most mantle (approximately 60–130 km depth range), which coincide with the location of the low attenuation anomaly observed in our study. In Figure 5a we plotted the *P*-wave velocity tomography results obtained by Golos et al. (2020) at the 50 km depth to examine the correlation of *P*-wave velocity and attenuation. Patches of relatively high-velocity anomalies are observed near the location of low-attenuation anomaly in the GoM Coastal Plain (Area D). Using seismic ambient noise recorded across the contiguous U.S., Bensen et al. (2008) produce shear wave tomographic dispersion images. At the period of 60 s, Rayleigh wave phase speed possesses sensitivity to the upper mantle and displays high-velocity anomalies along the northern border of the GoM Coastal Plain and agrees well with our attenuation results (Figure 5b). Similarly, in the period range of 40–60 s, Gaite et al. (2012) obtain high-velocity anomalies in the SEUS using seismic ambient noise data. Another high resolution 3-D shear velocity model of the crust and uppermost mantle beneath Mexico and the southern U.S., constrained by Rayleigh wave group velocity measurements up to 90 s period, reveals higher seismic velocities in the SEUS relative to the southwestern U.S. in the uppermost mantle (Spica et al., 2016).

4.2. Spatial Variations of Scattering

Scattering is an important factor that can lead to the decay of the amplitude because of the heterogeneity of the Earth's crust and mantle (Shapiro & Kneib, 1993). Most of the rocks and minerals contain heterogeneities in the form of grains, mineral boundaries, pore edges, cracks, etc., and the seismic energy is scattered when it encounters these features. Different modes of scattering are often determined based on the ratio between the scale of heterogeneity of the medium, a, and the wavelength (Wu & Aki, 1985).

$$S_r = 2\pi a \ / \ \text{wavelength}. \tag{8}$$

A small S_r (<<0.01) indicates that the size of the heterogeneities is extremely small relative to the seismic wavelength, leading to insignificant scattering. Scattering from heterogeneities with $0.01 < S_r < 0.1$ is termed as Rayleigh scattering, and that from heterogeneities with S_r in the range of 0.1 and 10 is termed as Mie scattering, which produces strong attenuation and distinguishable scattering in the seismic signal.

Theoretically, there should be zero energy on the transverse component of *P*-waves in an isotropic medium that is free of heterogeneities capable of producing scattering. Therefore, most of the energy in the *P*-wave window on the transverse component is the scattered energy due to 3-D heterogeneity. To examine the lateral variation of the strength of scattering, we calculated the ratio of the mean absolute amplitude between the transverse component and that of the vertical component for all the events that we used to estimate the Δt*. We selected a signal window that is 5 s before and 10 s after, and a noise window that is 5–15 s before, the theoretical *P*-wave arrival time for both the vertical and transverse components. A bandpass filter with

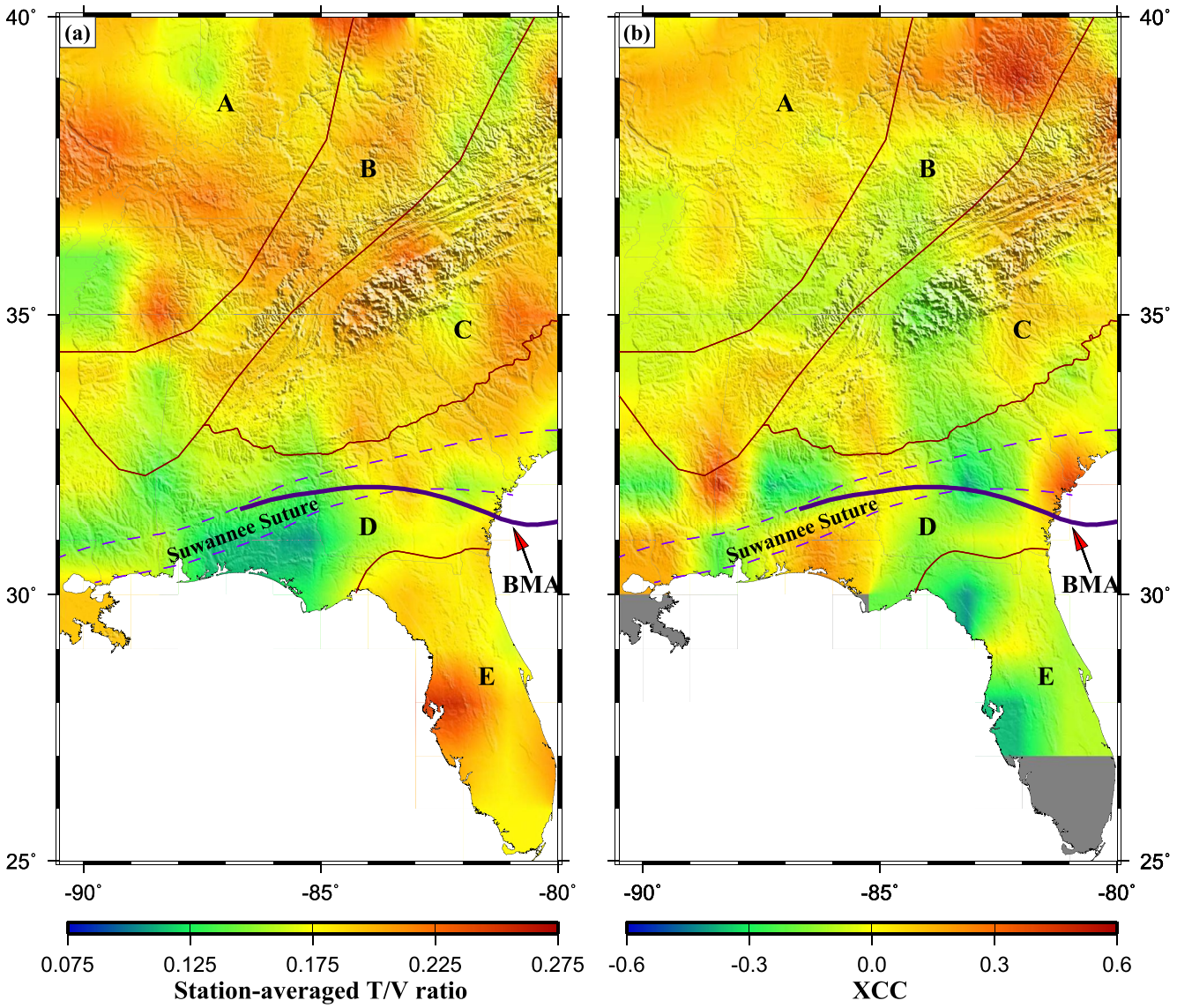

Figure 8. (a) Station-averaged transverse/vertical amplitude ratios. (b) Cross-correlation coefficient between individual Δt* measurements and transverse/vertical amplitude ratios at each station. The tectonic and sub-regional boundaries are the same as those shown in Figure 5.

corner frequencies of 0.1 and 0.5 Hz is used, which is identical to the one used in Δt* calculation. The ratio of the noise normalized absolute mean amplitude between the transverse and vertical components is calculated for each of the event-station pairs using

$$Rtz = \frac{Ts \ / \ Tn}{Zs \ / \ Zn}, \tag{9}$$

where Z_s and T_s are the mean absolute vertical and transverse amplitudes in the signal window, and, Z_n and T_n are the mean absolute vertical and transverse amplitudes in the noise window, respectively.

The station-averaged *Rtz* measurements for the entire study area (Figure 8a) range from 0.086 to 0.424, with a mean value of 0.187 ± 0.040 s. The GoM Coastal Plain, which is an area characterized by low attenuation anomalies (Figure 5b), is dominated by low *Rtz* values. Patches of relatively high *Rtz* values are observed in the Appalachian Plateau, and the southwestern part of the Floridan Peninsula. To examine the intensity of scattering across the SEUS, we calculated the cross-correlation coefficient (XCC) between individual Δt*

and *Rtz* measurements. A strong positive correlation between Δt* and *Rtz* values would reveal potential scattering artifacts, and zero or negative correlation would indicate that the Δt* values likely reflect intrinsic attenuation (Cafferky & Schmandt, 2015). High positive XCCs are observed near the Appalachian Mountains and northwest part of the Appalachian Plateau (Figure 8b), which is consistent with the scattering estimates obtained by Cafferky & Schmandt (2015) from T/Z spectral analysis of teleseismic *P*-waves in the frequency between 0.08 and 0.4 Hz. Using receiver function, Schulte-Pelkum & Mahan (2014) report high scattering in the Appalachian Mountains. A recent study that uses the USArray data to estimate the crustal attenuation of high frequency (1–20 Hz) shear waves reports high scattering in parts of Interior Plains and Appalachian Highlands (Eulenfeld & Wegler, 2017). They also report low scattering in the parts of the GoM Coastal Plain including the Lower Mississippi Region. The relatively low *Rtz* values and mostly negative XCCs observed along the GoM Coastal Plain in our study suggest a relatively more homogenous crustal and upper mantle structure in this area.

4.3. Geographical Variations and Geological Implications of Δt*

The geographic variation of Δt* across the SEUS provides insights into the structure and dynamics of the upper mantle. The estimated Δt* measurements correspond with the *P*-wave velocity anomalies in the uppermost mantle (Figure 5a). The strongest correspondences include high Δt* in the Appalachians, where upper mantle velocities are low, and low Δt* in the GoM Coastal Plain where an E-W strip of high upper mantle velocities are reported in numerous velocity tomography studies (Bensen et al., 2008; Biryol et al., 2016; Gaite et al., 2012; Golos et al., 2018; Spica et al., 2016). Previous seismic studies have revealed mantle upwelling beneath several sections of the Appalachians along the eastern North American margin (Savage et al., 2017; Schmandt & Lin, 2014), and some of which are attributed to edge-driven convection (Menke et al., 2016). A recent study (Byrnes et al., 2019) estimates the upper mantle seismic attenuation beneath the Appalachian Mountains using the tight station spacing of 10–25 km. They interpret the high-attenuating upper mantle as the result of the removal of mantle lithosphere from a 100 km wide region beneath the central Appalachian Mountains.

The low attenuation anomaly observed beneath the GoM Coastal Plain lies within the proposed Suwannee suture zone (Thomas, 2011), and roughly coincides with the east-west trending BMA (Figure 5b) (Higgins & Zietz, 1983; Mueller et al., 2014; Williams & Hatcher, 1983). This magnetic anomaly located within the study area runs from Alabama across southern Georgia up to North Carolina's northern banks in the Atlantic Ocean. The source of the BMA is ambiguous because of its apparent connection with both the Permo-Carboniferous Alleghanian orogeny (330–270 Ma) and the volcanic rocks that caused the emplacement of the Central Atlantic Magmatic Province (~200 Ma). Lower crustal seismic reflectors overlapping the location of magnetic low in southern Georgia (McBride & Nelson, 1988) and more recent magnetic models (Parker, 2014) suggest that the continental segment of the BMA can be explained by the collision of Laurentia and Gondwana. Seismic data have revealed the remnants of Pangea's breakup in the shallow crust near the BMA, providing evidence for the collision zone in the deep crust (Parker, 2014). Therefore, the low attenuation anomaly along the path of BMA can be explained by the presence of remnant lithospheric fragments in the deep crust or the uppermost mantle.

S-to-P receiver function studies using the USArray data (e.g., Hopper & Fischer, 2018; Liu & Gao, 2018) suggest that in the SEUS, the lithosphere has an average thickness of ~70 km, which is comparable to the estimated optimal depth of the weighted center of the anomalous attenuation layer (Figure 7). In addition, seismic tomography studies suggest a high velocity band approximately overlaps with the low attenuation zone along the GoM Coastal Plain in the depth range of ~20–~200 km relative to the Appalachians (Golos et al., 2020). Using the Qp values in the PREM model (Dziewonski & Anderson, 1981) for the remnant lithosphere ($Q_L = 1400$) and the surrounding asthenosphere ($Q_A = 195$), and Vp values of 8.1 km/s for the lithosphere (V_L) and 8.0 km/s for the asthenosphere (V_A), respectively, the required vertical length of the remnant lithospheric slab (R_L) in order to produce the observed −0.17 s ± 0.02 Δt* value is as large as 305 ± 35 km which is inconsistent with results from seismic tomography studies. One way to produce a more reasonable R_L is to use a smaller Q_A value. For instance, when a Q_A value of 120 is used, R_L would reduce to ~180 ± 20 km which is more in accordance with tomography results (e.g., Golos et al., 2020). Additional studies are needed to isolate the intrinsic attenuation from the observed total Δt* and to more

accurately determine the absolute *Qp* value for the proposed lithospheric segments and that of the ambient asthenosphere, in order to confirm the existence of the lithospheric segments and their spatial distribution.

5. Conclusions

We have utilized 14,702 teleseismic *P*-wave amplitude spectra recorded by 477 broadband seismic stations to map the spatial distribution of Δt* in the SEUS. This large data set of events recorded by the dense array of stations including 220 USArray TA stations provides a better constraint on the crustal and upper mantle *P*-wave attenuation structure than previous larger-scale attenuation studies. The resulting Δt* measurements show a systematic contrast between the Appalachian Mountain range and the GoM Coastal Plain exhibiting high and low attenuation, respectively. An east-west strip of low attenuation anomaly is identified beneath most of the GoM Coastal Plain. The weighted center of this anomaly is located at about 70 km depth as estimated using the spatial coherency approach. This anomaly lies along the Suwannee suture zone that separated Laurentia and Gondwana during the Alleghanian orogeny. It also coincides with the path of the Brunswick Magnetic anomaly, providing evidence of low attenuation and fast velocity bodies in the upper-most mantle that are likely remnant lithospheric segments extending from the crust to the middle upper mantle. The ratio between the transverse and vertical amplitudes of the *P*-wave is calculated to estimate the lateral variation of scattering. Areas of relatively high transverse/vertical ratios are observed in the Appalachian Plateau and the Floridan Peninsula, whereas low ratios observed in the GoM Coastal Plain indicate that this area is relatively less capable of producing scattering.

Data Availability Statement

Station and event information, the measured Δt* and its standard deviation (SD), as well as a plot similar to Figure 3 for each of the 14,702 measurements obtained in this study, can be found at https://web.mst.edu/~as6g7/1g_SEUS_tst/. All the seismic waveform data used in this study were freely available from the Incorporated Research Institutions for Seismology Data Management Center (https://ds.iris.edu/ds/nodes/dmc/data/types/waveform-data/; last accessed: January 2019) under the main network codes of 6E (https://doi.org/10.7914/SN/6E_2013), IM (International Miscellaneous Stations), IU (https://doi.org/10.7914/SN/IU), N4 (https://doi.org/10.7914/SN/N4), NM (Cooperative New Madrid Seismic Network), PN (PEPP-Indiana), SP (https://doi.org/10.7914/SN/SP), TA (https://doi.org/10.7914/SN/TA), US (https://doi.org/10.7914/SN/US), XO (https://doi.org/10.7914/SN/XO_2011), XR (https://doi.org/10.7914/SN/XR_2001), and Z9 (https://doi.org/10.7914/SN/Z9_2010).

Acknowledgments
The study was partially supported by the U.S. National Science Foundation under Grant No. 1919789. We thank two anonymous reviewers and Editor Maureen Long for providing thoughtful and constructive feedbacks that significantly improved the manuscript.

References

Aki, K. (1980). Attenuation of shear-waves in the lithosphere for frequencies from 0.05 to 25 Hz. *Physics of the Earth and Planetary Interiors*, *21*(1), 50–60. https://doi.org/10.1016/0031-9201(80)90019-9

Akinci, A., Pezzo, del, E., & Ibáñez, J. M. (1995). Separation of scattering and intrinsic attenuation in southern Spain and western Anatolia (Turkey). *Geophysical Journal International*, *121*(2), 337–353. https://doi.org/10.1111/j.1365-246X.1995.tb05715.x

Anderson, D. L. (1967). The anelasticity of the mantle. *Geophysical Journal International*, *14*(1–4), 135–163. https://doi.org/10.1111/j.1365-246X.1967.tb06232.x

Bao, X., Dalton, C. A., Jin, G., Gaherty, J. B., & Shen, Y. (2016). Imaging Rayleigh wave attenuation with USArray. *Geophysical Journal International*, *206*(1), 241–259. https://doi.org/10.1093/gji/ggw151

Baqer, S., & Mitchell, B. J. (1999). Regional variation of Lg coda Q in the continental United States and its relation to crustal structure and evolution. In B. J. Mitchell, & B. Romanowicz (Eds.), Q of the Earth: Global, regional, and laboratory studies (pp. 613–638). Birkhäuser. https://doi.org/10.1007/978-3-0348-8711-3_17

Bensen, G. D., Ritzwoller, M. H., & Shapiro, N. M. (2008). Broadband ambient noise surface wave tomography across the United States. *Journal of Geophysical Research*, *113*, B05306. https://doi.org/10.1029/2007JB005248

Biryol, C. B., Wagner, L. S., Fischer, K. M., & Hawman, R. B. (2016). Relationship between observed upper mantle structures and recent tectonic activity across the Southeastern United States. *Journal of Geophysical Research: Solid Earth*, *121*(5), 3393–3414. https://doi.org/10.1002/2015JB012698

Byrnes, J. S., Bezada, M., Long, M. D., & Benoit, M. H. (2019). Thin lithosphere beneath the central Appalachian Mountains: Constraints from seismic attenuation beneath the MAGIC array. *Earth and Planetary Science Letters*, *519*, 297–307. https://doi.org/10.1016/j.epsl.2019.04.045

Cafferky, S., & Schmandt, B. (2015). Teleseismic P wave spectra from USArray and implications for upper mantle attenuation and scattering. *Geochemistry, Geophysics, Geosystems*, *16*(10), 3343–3361. https://doi.org/10.1002/2015GC005993

Cook, F. A., Albaugh, D. S., Brown, L. D., Kaufman, S., Oliver, J. E., & Hatcher, R. D. (1979). Thin-skinned tectonics in the crystalline southern Appalachians; COCORP seismic-reflection profiling of the Blue Ridge and Piedmont. *Geology*, *7*(12), 563–567. https://doi.org/10.1130/0091-7613(1979)7<563:TTITCS>2.0.CO;2

Deen, T. J., Griffin, W. L., Begg, G., O'Reilly, S. Y., Natapov, L. M., & Hronsky, J. (2006). Thermal and compositional structure of the subcontinental lithospheric mantle: Derivation from shear wave seismic tomography. *Geochemistry, Geophysics, Geosystems*, *7*(7). https://doi.org/10.1029/2005GC001120

Denison, R. E., Lidiak, E. G., Bickford, M. E., & Kisvarsanyi, E. B. (1984). *Geology and geochronology of Precambrian rocks in the Central Interior region of the United States*. In Professional Paper. USGS.

Der, Z. A., & McElfresh, T. W. (1976). Short-period P-wave attenuation along various paths in North America as determined from P-wave spectra of the SALMON nuclear explosion. *Bulletin of the Seismological Society of America*, *66*(5), 1609–1622.

Der, Z. A., & McElfresh, T. W. (1977). The relationship between anelastic attenuation and regional amplitude anomalies of short-period P waves in North America. *Bulletin of the Seismological Society of America*, *67*(5), 1303–1317.

Der, Z. A., McElfresh, T. W., & O'Donnell, A. (1982). An investigation of the regional variations and frequency dependence of anelastic attenuation in the mantle under the United States in the 0.5–4 Hz band. *Geophysical Journal International*, *69*(1), 67–99. https://doi.org/10.1111/j.1365-246X.1982.tb04936.x

Dong, M. T., & Menke, W. H. (2017). Seismic high attenuation region observed beneath southern New England from teleseismic body wave spectra: Evidence for high asthenospheric temperature without melt. *Geophysical Research Letters*, *44*(10), 958–969. https://doi.org/10.1002/2017GL074953

Dziewonski, A. M. (1979). Elastic and anelastic structure of the Earth. *Reviews of Geophysics*, *17*(2), 303–312. https://doi.org/10.1029/RG017i002p00303

Dziewonski, A. M., & Anderson, D. L. (1981). Preliminary reference Earth model. *Physics of the Earth and Planetary Interiors*, *25*(4), 297–356. https://doi.org/10.1016/0031-9201(81)90046-7

Eulenfeld, T., & Wegler, U. (2017). Crustal intrinsic and scattering attenuation of high-frequency shear waves in the contiguous United States. *Journal of Geophysical Research: Solid Earth*, *122*, 4676–4690. https://doi.org/10.1002/2017JB014038

Faul, U. H., & Jackson, I. (2005). The seismological signature of temperature and grain size variations in the upper mantle. *Earth and Planetary Science Letters*, *234*(1), 119–134. https://doi.org/10.1016/j.epsl.2005.02.008

Gaite, B., Iglesias, A., Villasenor, A., Herraiz, M., & Pacheco, J. F. (2012). Crustal structure of Mexico and surrounding regions from seismic ambient noise tomography. *Geophysical Journal International*, *188*(3), 1413–1424. https://doi.org/10.1111/j.1365-246X.2011.05339.x

Gallegos, A., Ranasinghe, N., Ni, J., & Sandvol, E. (2014). Lg attenuation in the central and eastern United States as revealed by the EarthScope transportable array. *Earth and Planetary Science Letters*, *402*, 187–196. https://doi.org/10.1016/j.epsl.2014.01.049

Gao, S. S. (1997). A Bayesian nonlinear inversion of seismic body-wave attenuation factors. *Bulletin of the Seismological Society of America*, *87*(4), 961–970.

Gao, S. S., & Liu, K. H. (2012). AnisDep: A FORTRAN program for the estimation of the depth of anisotropy using spatial coherency of shear-wave splitting parameters. *Computers & Geosciences*, *49*, 330–333. https://doi.org/10.1016/j.cageo.2012.01.020

Gladwin, M. T., & Stacey, F. D. (1974). Anelastic degradation of acoustic pulses in rock. *Physics of the Earth and Planetary Interiors*, *8*(4), 332–336. https://doi.org/10.1016/0031-9201(74)90041-7

Godey, S., Deschamps, F., Trampert, J., & Snieder, R. (2004). Thermal and compositional anomalies beneath the North American continent. *Journal of Geophysical Research*, *109*(B1). https://doi.org/10.1029/2002JB002263

Goes, S., Govers, R., & Vacher, P. (2000). Shallow mantle temperatures under Europe from P and S wave tomography. *Journal of Geophysical Research*, *105*(B5), 11153–11169. https://doi.org/10.1029/1999JB900300

Goes, S., & Lee, van der, S. (2002). Thermal structure of the North American uppermost mantle inferred from seismic tomography. *Journal of Geophysical Research*, *107*(B3), ETG-2-1–ETG-2-13. https://doi.org/10.1029/2000JB000049

Golos, E., Fang, H., & Hilst, van der, R. D. (2020). Variations in seismic wave speed and Vp/Vs ratio in the North American lithosphere. *Journal of Geophysical Research: Solid Earth*, *125*, e2020JB020574. https://doi.org/10.1029/2020JB020574

Golos, E. M., Fang, H., Yao, H., Zhang, H., Burdick, S., Vernon, F., et al. (2018). Shear wave tomography beneath the United States using a joint inversion of surface and body waves. *Journal of Geophysical Research: Solid Earth*, *123*(6), 5169–5189. https://doi.org/10.1029/2017JB014894

Gorich, U., & Muller, G. (1987). Apparent and intrinsic Q: The one-dimensional case. *Journal of Geophysics*, *61*(1), 46–54.

Grand, S. P., & Helmberger, D. V. (1984). Upper mantle shear structure of North America. *Geophysical Journal International*, *76*(2), 399–438. https://doi.org/10.1111/j.1365-246X.1984.tb05053.x

Halderman, T. P., & Davis, P. M. (1991). Qp beneath the Rio Grande and East African rift zones. *Journal of Geophysical Research*, *96*(B6), 10113. https://doi.org/10.1029/91jb00146

Hatcher, R. D. (2010). *The appalachian orogen: A brief summary*. In: From Rodinia to Pangea: The lithotectonic record of the appalachian region. Geological Society of America. https://doi.org/10.1130/2010.1206(01)

Higgins, M. W., & Zietz, I. (1983). Geologic interpretation of geophysical maps of the pre-Cretaceous "basement" beneath the Coastal Plain of the Southeastern United States. In: Geological Society of America Memoirs (Vol. 158, pp. 125–130). Geological Society of America. https://doi.org/10.1130/mem158-p125

Hopper, E., & Fischer, K. M. (2018). The changing face of the lithosphere–asthenosphere boundary: Imaging continental scale patterns in upper mantle structure across the contiguous U.S. with Sp converted waves. *Geochemistry, Geophysics, Geosystems*, *19*(8), 2593–2614. https://doi.org/10.1029/2018GC007476

Hwang, Y. K., Ritsema, J., & Goes, S. (2009). Spatial variations of P wave attenuation in the mantle beneath North America. *Journal of Geophysical Research*, *114*(B6). https://doi.org/10.1029/2008JB006091

Iverson, W. P., & Smithson, S. B. (1983). Reprocessing and reinterpretation of COCORP southern Appalachian profiles. *Earth and Planetary Science Letters*, *62*(1), 75–90. https://doi.org/10.1016/0012-821X(83)90072-9

Jackson, D. D., & Anderson, D. L. (1970). Physical mechanisms of seismic-wave attenuation. *Reviews of Geophysics*, *8*(1), 1–63. https://doi.org/10.1029/RG008i001p00001

Jackson, I., Gerald, J. D. F., Faul, U. H., & Tan, B. H. (2002). Grain-size-sensitive seismic wave attenuation in polycrystalline olivine. *Journal of Geophysical Research*, *107*(B12), ECV-5-1–ECV-5-16. https://doi.org/10.1029/2001JB001225

Jannsen, D., Voss, J., & Theilen, F. (1985). Comparison of methods to determine Q in shallow marine sediments from vertical reflection seismograms. *Geophysical Prospecting*, *33*(4), 479–497. https://doi.org/10.1111/j.1365-2478.1985.tb00762.x

Karato, S. (1993). Importance of anelasticity in the interpretation of seismic tomography. *Geophysical Research Letters*, *20*(15), 1623–1626. https://doi.org/10.1029/93GL01767

Kennett, B. L. N., & Engdahl, E. R. (1991). Traveltimes for global earthquake location and phase identification. *Geophysical Journal International*, *105*(2), 429–465. https://doi.org/10.1111/j.1365-246X.1991.tb06724.x

Knopoff, L. (1964). Q. *Reviews of Geophysics*, *2*(4), 625–660. https://doi.org/10.1029/RG002i004p00625

Kovach, R. L., & Anderson, D. L. (1964). Attenuation of shear waves in the upper and lower mantle. *Bulletin of the Seismological Society of America*, *54*(6A), 1855–1864.
Lawrence, J. F., Shearer, P. M., & Masters, G. (2006). Mapping attenuation beneath North America using waveform cross-correlation and cluster analysis. *Geophysical Research Letters*, *33*(7), L07315. https://doi.org/10.1029/2006GL025813
Lee, C.-T. A. (2003). Compositional variation of density and seismic velocities in natural peridotites at STP conditions: Implications for seismic imaging of compositional heterogeneities in the upper mantle. *Journal of Geophysical Research*, *108*(B9). https://doi.org/10.1029/2003JB002413
Liu, K. H., & Gao, S. S. (2010). Spatial variations of crustal characteristics beneath the Hoggar swell, Algeria, revealed by systematic analyses of receiver functions from a single seismic station. *Geochemistry, Geophysics, Geosystems*, *11*, Q08011. https://doi.org/10.1029/2010GC003091
Liu, K. H., & Gao, S. S. (2011). Estimation of the depth of anisotropy using spatial coherency of shear-wave splitting parameters. *Bulletin of the Seismological Society of America*, *101*(5), 2153–2161. https://doi.org/10.1785/0120100258
Liu, L., & Gao, S. S. (2018). Lithospheric layering beneath the contiguous United States constrained by S-to-P receiver functions. *Earth and Planetary Science Letters*, *495*, 79–86. https://doi.org/10.1016/j.epsl.2018.05.012
Marone, F., & Romanowicz, B. (2007). Non-linear crustal corrections in high-resolution regional waveform seismic tomography. *Geophysical Journal International*, *170*(1), 460–467. https://doi.org/10.1111/j.1365-246X.2007.03399.x
McBride, J., & Nelson, K. (1988). Integration of COCORP deep reflection and magnetic anomaly analysis in the southeastern United States: Implications for origin of the Brunswick and East Coast magnetic anomalies. *Geological Society of America Bulletin*, *100*, 436–445. https://doi.org/10.1130/0016-7606(1988)100<0436:IOCDRA>2.3.CO;2
Melbourne, T., & Helmberger, D. (1998). Fine structure of the 410-km discontinuity. *Journal of Geophysical Research*, *103*(B5), 10091–10102. https://doi.org/10.1029/98JB00164
Menke, W., Skryzalin, P., Levin, V., Harper, T., Darbyshire, F., & Dong, T. (2016). The Northern Appalachian Anomaly; a modern asthenospheric upwelling. *Geophysical Research Letters*, *43*(10), 173–179. https://doi.org/10.1002/2016GL070918
Mueller, P. A., Heatherington, A. L., Foster, D. A., Thomas, W. A., & Wooden, J. L. (2014). The Suwannee suture: Significance for Gondwana-Laurentia terrane transfer and formation of Pangaea. *Gondwana Research*, *26*(1), 365–373. https://doi.org/10.1016/j.gr.2013.06.018
Parker, E. H., Jr. (2014). Crustal magnetism, tectonic inheritance, and continental rifting in the southeastern United States. *Geological Society of America Today*, *24*(4), 4–9. https://doi.org/10.1130/GSAT-G192A.1
Pasyanos, M. E. (2013). A lithospheric attenuation model of North America. *Bulletin of the Seismological Society of America*, *103*(6), 3321–3333. https://doi.org/10.1785/0120130122
Raikes, S. A., & White, R. E. (1984). Measurements of Earth attenuation from downhole and surface seismic recordings. *Geophysical Prospecting*, *32*(5), 892–919. https://doi.org/10.1111/j.1365-2478.1984.tb00745.x
Rankin, D. W., Dillon, W. P., Black, D. F. B., Boyer, S. E., Daniels, D. L., Goldsmith, R., et al. (1991). *E-4 Central Kentucky to the Carolina trough*. Geological Society of America. https://doi.org/10.1130/DNAG-COT-E-4
Sato, H., Sacks, I. S., & Murase, T. (1989). The use of laboratory velocity data for estimating temperature and partial melt fraction in the low-velocity zone: Comparison with heat flow and electrical conductivity studies. *Journal of Geophysical Research*, *94*(B5), 5689–5704. https://doi.org/10.1029/JB094iB05p05689
Savage, B., Covellone, B. M., & Shen, Y. (2017). Wave speed structure of the eastern North American margin. *Earth and Planetary Science Letters*, *459*, 394–405. https://doi.org/10.1016/j.epsl.2016.11.028
Schmandt, B., & Lin, F.-C. (2014). P and S wave tomography of the mantle beneath the United States. *Geophysical Research Letters*, *41*, 2014GL061231. https://doi.org/10.1002/2014GL061231
Schulte-Pelkum, V., & Mahan, K. H. (2014). A method for mapping crustal deformation and anisotropy with receiver functions and first results from USArray. *Earth and Planetary Science Letters*, *402*, 221–233. https://doi.org/10.1016/j.epsl.2014.01.050
Schutt, D. L., & Lesher, C. E. (2006). Effects of melt depletion on the density and seismic velocity of garnet and spinel lherzolite. *Journal of Geophysical Research*, *111*(B5). https://doi.org/10.1029/2003JB002950
Shapiro, N. M., & Ritzwoller, M. H. (2004). Inferring surface heat flux distributions guided by a global seismic model: Particular application to Antarctica. *Earth and Planetary Science Letters*, *223*(1), 213–224. https://doi.org/10.1016/j.epsl.2004.04.011
Shapiro, S. A., & Kneib, G. (1993). Seismic attenuation by scattering: Theory and numerical results. *Geophysical Journal International*, *114*, 373–391. https://doi.org/10.1111/j.1365-246X.1993.tb03925.x
Shen, W., & Ritzwoller, M. H. (2016). Crustal and uppermost mantle structure beneath the United States. *Journal of Geophysical Research: Solid Earth*, *121*(6), 4306–4342. https://doi.org/10.1002/2016JB012887
Sobolev, S., Zeyen, H., Stoll, G., Werling, F., Altherr, R., & Fuchs, K. (1996). Upper mantle temperatures from teleseismic tomography of French Massif Central including effects of composition, mineral reactions, anharmonicity, anelasticity and partial melt. *Earth and Planetary Science Letters*, *139*(1), 147–163. https://doi.org/10.1016/0012-821X(95)00238-8
Solomon, S. C. (1972). Seismic-wave attenuation and partial melting in the upper mantle of North America. *Journal of Geophysical Research*, *77*(8), 1483–1502. https://doi.org/10.1029/JB077i008p01483
Solomon, S. C., & Toksöz, M. N. (1970). Lateral variation of attenuation of P and S waves beneath the United States. *Bulletin of the Seismological Society of America*, *60*(3), 819–838.
Spica, Z., Perton, M., Calo, M., Legrand, D., Cordoba-Montiel, F., & Iglesias, A. (2016). 3-D shear wave velocity model of Mexico and South US: Bridging seismic networks with ambient noise cross-correlations (C^1) and correlation of coda of correlations (C^3). *Geophysical Journal International*, *206*(3), 795–1813. https://doi.org/10.1093/gji/ggw240
Swaby, A. N., Lucas, M. D., & Ross, R. M. (2016). *The teacher-friendly guide to the earth science of the southeastern US* (2nd ed., p. 460). Ithaca: Paleontological Research Institution.
Swann, D. H. (1968). *A summary geologic history of the Illinois Basin in Geology and petroleum production of the Illinois basin* (pp. 3–21). Illinois Geologic Society.
Taner, M. T., Koehler, F., & Sheriff, R. E. (1979). Complex seismic trace analysis. *Geophysics*, *44*(6), 1041–1063. https://doi.org/10.1190/1.1440994
Teng, T.-L. (1968). Attenuation of body waves and the Q structure of the mantle. *Journal of Geophysical Research*, *73*(6), 2195–2208. https://doi.org/10.1029/JB073i006p02195
Thomas, M. D. (1985). Gravity studies of the Grenville Province: Significance for Precambrian plate collision and the origin of anorthosite. In: The utility of regional gravity and magnetic anomaly maps (pp. 109–123). Society of Exploration Geophysicists. https://doi.org/10.1190/1.0931830346.ch10

Thomas, W. A. (2006). Tectonic inheritance at a continental margin. *Geological Society of America*, *16*(2). https://doi.org/10.1130/1052-5173(2006)016[4:tiaacm]2.0.co;2

Thomas, W. A. (2011). The Iapetan rifted margin of southern Laurentia. *Geosphere*, *7*(1), 97–120. https://doi.org/10.1130/GES00574.1

van der Lee, S., & Nolet, G. (1997). Upper mantleSvelocity structure of North America. *Journal of Geophysical Research: Solid Earth*, *102*(B10), 22815–22838. https://doi.org/10.1029/97jb01168

van der Pluijm, B. A., & Catacosinos, P. A. (1996). Basement and basins of eastern North America. *Geological Society of America*, *308*, 14. https://doi.org/10.1130/SPE308

van Schmus, W. R., Schneider, D. A., Holm, D. K., Dodson, S., & Nelson, B. K. (2007). New insights into the southern margin of the Archean-Proterozoic boundary in the north-central United States based on U-Pb, Sm-Nd, Ar-Ar geochronology. *Precambrian Research*, *157*, 80–105. https://doi.org/10.1016/j.precamres.2007.02.011

Wang, H., Zhao, D., Huang, Z., & Wang, L. (2019). Tomography, seismotectonics, and mantle dynamics of Central and Eastern United States. *Journal of Geophysical Research: Solid Earth*, *124*(8), 8890–8907. https://doi.org/10.1029/2019JB017478

Wang, Z., Zhao, D., Liu, X., & Li, X. (2017). Seismic attenuation tomography of the source zone of the 2016 Kumamoto earthquake (M 7.3). *Journal of Geophysical Research: Solid Earth*, *122*(4), 2988–3007. https://doi.org/10.1002/2016JB013704

Williams, H., & Hatcher, R. D. (1983). Appalachian suspect terranes. In: Geological Society of America Memoirs (Vol. 158, pp. 33–53). Geological Society of America. https://pubs.geoscienceworld.org/books/book/168/chapter/3791953/

Wu, R., & Aki, K. (1985). Scattering characteristics of elastic waves by an elastic heterogeneity. *Geophysics*, *50*(4), 582–595. https://doi.org/10.1190/1.1441934